Desalination and Water Treatment
www.deswater.com

doi: 10.5004/dwt.2020.25709

190 (2020) 256–266
June

Acylamino functionalized triazine-based porous organic polymers for efficient Cd^{2+} capture

Aiping Hao[a], Rongxin Peng[b], Jianhan Huang[b,*]

[a]*College of Chemistry and Materials, Hunan University of Arts and Science, Changde, 415000, China, email: 421471398@qq.com (A. Hao)*
[b]*College of Chemistry and Chemical Engineering, Central South University, Changsha, 410083, China, emails: jianhanhuang@csu.edu.cn (J. Huang), 1411834410@qq.com (R. Peng)*

Received 22 August 2019; Accepted 12 February 2020

ABSTRACT

Functionalized porous organic polymers (POPs) with high Brunauer–Emmett–Teller surface area (S_{BET}) are promising for the removal of heavy metals while their synthesis remains a challenge. A kind of acylamino functionalized triazine-based POPs was developed from melamine and trimesic acid by one-pot polycondensation in this study. The resultant polymers were applied for Cd^{2+} removal from aqueous solution. These polymers had controllable S_{BET} of 246–463 m^2/g with the predominant mesoporous distribution. Due to their well-constructed porosity and plentiful acylamino groups, they were efficient for Cd^{2+} removal with the maximum capacity of 392.5 mg/g at pH = 6. The adsorption was very fast and less than 15 min was enough to attain the equilibrium. Analysis of the mechanism revealed that the embedded acylamino and triazine ring played a role due to the strong chelating of the oxygen and nitrogen with Cd^{2+}.

Keywords: Triazine; Porous organic polymers (POPs); Adsorption

1. Introduction

Cadmium (Cd^{2+}) pollution is a severe environmental problem due to its high toxicity and accumulative character [1,2]. Cd^{2+} is difficult to be degraded in nature and it can be continuously enriched in living organisms, which seriously threatens human health and ecological environment [3]. The maximum emission standard of Cd^{2+} is 5 μg/L in drinking water by the Environmental Protection Agency of the United States, and less than 3 μg/L of Cd^{2+} can exist by the World Health Organization. Thus, efficient removal of Cd^{2+} is urgent while still remains a challenge [4,5]. Various methods including chemical precipitation, ion exchange, and adsorption are applied for Cd^{2+} removal [6–8], and adsorption by solid materials is identified as the most popular method due to its operation simplicity, high efficiency, and easy recovery [9,10].

Many solid materials including low-cost sorbents [11], mesoporous silica [12], activated carbon [13–15], nano-particles [16,17], graphene oxide [18,19], and porous organic polymers (POPs) [20–22] are fabricated for Cd^{2+} removal. The POPs have attracted increasing attention due to their high Brunauer–Emmett–Teller (BET) surface area (S_{BET}), outstanding porosity, and diversified chemical structure [23]. Their molecular structure is flexibly designed to assemble different architectures. Moreover, their post-functionalization by introducing various functional groups can be easily realized [24,25], giving more active sites for strong interaction of heavy metal ions. Cd^{2+} tends to form a stable covalent bond with S/N-containing functional groups such as $–NH_2$, COOH, and –SH [26–28]. Thus, these specific groups are often introduced on the POPs. The results indicate that the Cd^{2+} adsorption is greatly enhanced due to the strong chelating between the heteroatoms (S and N) and Cd^{2+} [29].

* Corresponding author.

Zhao et al. [30] prepared the magnetic Schiff-based POPs for Cd^{2+} removal and the maximum capacity (q_{max}) arrived at 0.8 mmol/g. Zeng et al. [31] reported that the polyacrylic acid modified nanotrap exhibited the q_{max} of 406.6 mg/g at pH = 7 for Cd^{2+}. However, the synthetic procedure of the POPs often involves noble metal catalysts, harsh synthetic conditions, and toxic solvents.

More recently, one-pot synthesis of the POPs under mild condition is anticipated. Saleh et al. [32] prepared the acylamino functionalized POPs from trimesic acid (TMA) and *p*-phenylenediamine by one-pot polycondensation. Taskin et al. [33] reported a Schiff-based POPs from terephthaldehyde and melamine (MA) by a Schiff-based reaction, the introduced N acts as a productive functional ligand for Cu^{2+}. He et al. [34] synthesized a triazine and thiophene bifunctionalized POPs from the Friedel–Crafts reaction, the introduced N easily forms coordination complex with Cu^{2+}. For this purpose, in this study a simple one-pot amidation was carried out under mild condition (atmospheric pressure and catalyst-free) using MA and TMA as the monomers, and the synthesized triazine-based POPs were functionalized with the acylamino groups. The simple one-pot amidation offers several advantages such as free-catalysts, low-cost raw materials, and few by-products. In addition, it gives the as-prepared POPs with plentiful acylamino groups, which are beneficial for Cd^{2+} adsorption. The equilibrium and kinetic adsorption were investigated in detail using Cd^{2+} as the model heavy metal, and the adsorption mechanism was illustrated in detail.

2. Experimental section

2.1. Synthesis of the acylamino modified triazine-based POPs

The acylamino modified triazine-based POPs were synthesized according to the method in ref. [35]. MA and TMA were used as the monomers and a typical amidation was carried out under mild condition. In brief, 7, 14, or 21 mmol of MA and 7 mmol of TMA were dissolved in 35 mL of DMSO and the mixture was continuously stirred at 423 K for 72 h. The obtained off-white powders namely NTM1, NTM2, and NTM3 were placed in a vacuum and dried at 353 K.

2.2. Characterization of the polymers

The Fourier transform infrared (FT-IR) spectra of the polymers were detected by a Nicolet 6700 Fourier transform infrared spectrophotometer (Thermo Scientific Co., United States). Micromeritics ASAP 2020 surface area (Micromeritics, USA) was used to measure the pore structure of the polymers. CHNOS elemental (Vario Micro Cube, Germany) was used to investigate the elemental analysis (EA). The X-ray photoelectron spectroscopy (XPS) was detected via the Thermo ESCALAB spectrometer with an Al K-α source. A field emission scanning electron microscope (FESEM, Nova Nano SEM 230) operating was used to detect the morphologies of the polymers. High-resolution transmission electron microscopy (TEM) was conducted on an FEI Titan G2 60–300 microscope. The thermogravimetric analysis (TGA) of the polymers was measured by thermobalance (STA-499C, NETZSCH, UK). The Cd^{2+} concentration was determined by the TAS-990 atomic absorption spectrum (AAS).

2.3. Adsorption performance

The Cd^{2+} adsorption on the polymers was performed by mixing 0.02 g of the polymers in 50 mL of Cd^{2+} aqueous solution. The initial concentration of Cd^{2+} was in the range of 100–500 mg/L, the solution pH ranged at 2–10 was adjusted with 0.1 mol/L of HCl or NaOH. The adsorption was performed at 298, 308, and 318 K, respectively. The concentrations of Cd^{2+} before and after the adsorption were analyzed by AAS and the adsorption capacity was calculated as,

$$q_e = \left(C_0 - C_e\right) \times \frac{V}{W} \tag{1}$$

where q_e (mg/g) is the equilibrium capacity, C_0 and C_e represent the initial and equilibrium concentration (mg/L), respectively, V is the volume of the solution (L) and W is the mass of the polymers (g).

3. Results and discussion

3.1. Structural characterization of the polymers

The one-pot amidation based on the amino groups of MA and the carboxyl groups of TMA was performed for MA and TMA in this study. MA and TMA have multiple amino and carboxyl groups. As a result, the as-prepared polymers are functionalized with plentiful acylamino groups. In addition, considerable amino (from MA) and carboxyl groups (from TMA) also remain, they are beneficial for Cd^{2+} adsorption. The FT-IR spectrum in Fig. S1 shows that the vibrational bands at 1,549 and 1,481 cm^{-1} were ascribed to the C=N stretching of the triazine ring [29,35,36]. The strong vibration at 1,675 cm^{-1} was generated from the C=O stretching of the acylamino groups [27,36]. The contact angles (CA) of the polymers in Fig. S2 revealed that these polymers were hydrophilic with the CA less than 90°, and a higher feeding amount of TMA induced a less CA due to the higher hydrophilicity. The XPS spectrum in Fig. 1a exhibited that the polymer contained 47.2 wt.% of carbon (C), 42.2 wt.% of N, and 10.6 wt.% of oxygen (O). These data were similar to the elemental analysis (C: 34.6 wt.%, N: 40.9 wt.%, H: 5.2 wt.%, S: 2.4 wt.%, and hence O was calculated to be 16.9 wt.%). In particular, it is clear that the ratio of N/O was higher than 2, suggesting that considerable amino groups remained on the polymers. As different feeding amount of MA and TMA was fed in this reaction, a similar phenomenon was observed (Fig. S3 and Table S1). Additionally, the bands with the binding energies at 268, 400, and 530 eV were assigned to the C1s, N1s, and O1s, respectively [35]. The high-resolution C1s in Fig. 1b revealed that three peaks at 284.7, 286.5, and 287.7 eV corresponded to the C=O, C=N, and C=C configurations, respectively. The high-resolution N1s in Fig. 1c was divided into three peaks of the C=N (398.3 eV, 38.3 wt.%), $-NH_2$ (399.5 eV, 55.9 wt.%), and –NH– (405.3 eV, 5.8 wt.%) configurations, respectively [22,36]. The high-resolution O1s in

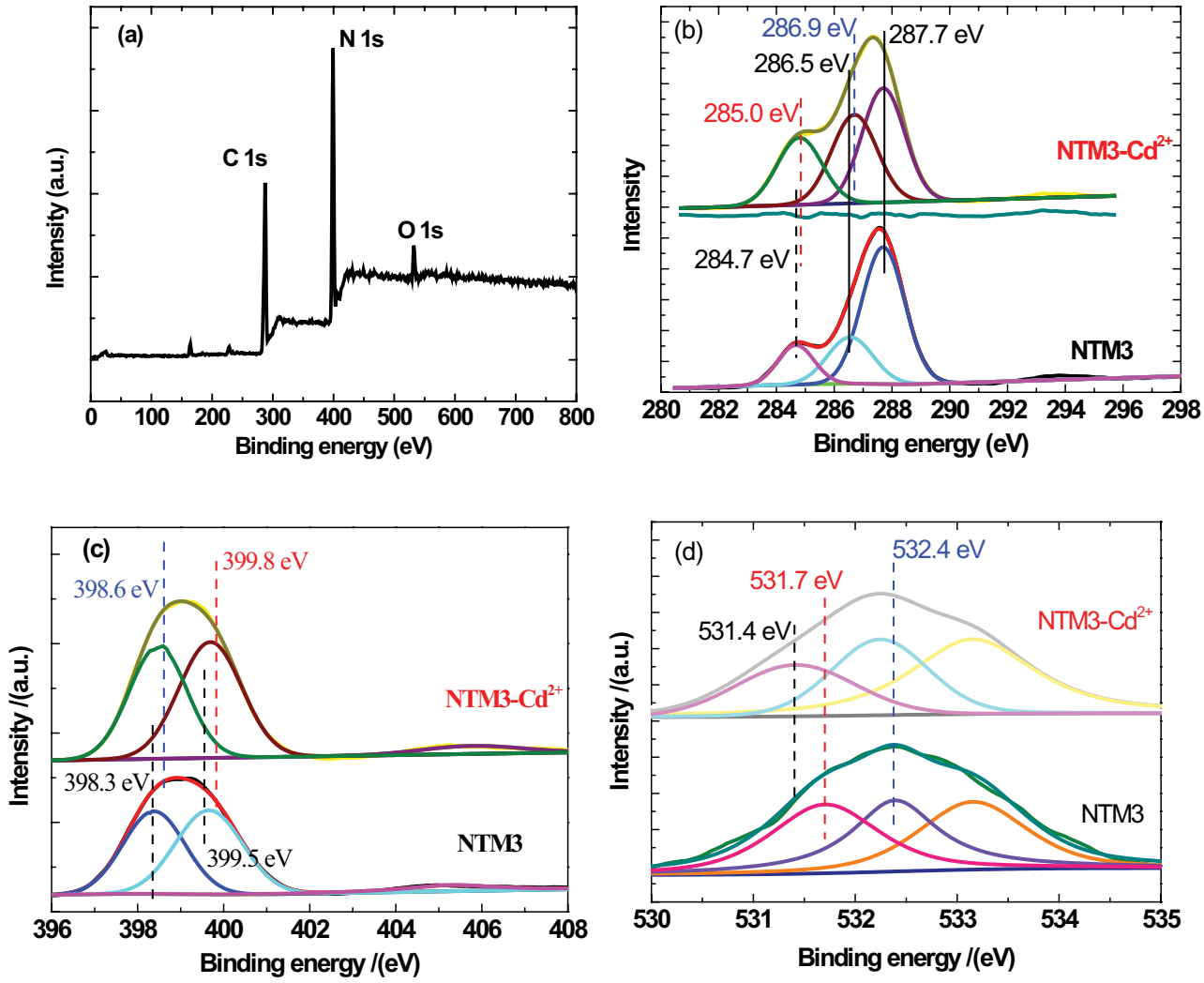

Fig. 1. XPS spectra of NTM3 (a) survey, (b) C1s and C1s-Cd^{2+}, (c) N1s and N1s-Cd^{2+}, and (d) O1s and O1s-Cd^{2+}.

Fig. 1d had the C=O (531.7 eV), C–O (532.4 eV), and H_2O (533.1 eV) configurations. The TGA in Fig. S4 indicated that the polymer was thermal stable. Less than 10 wt.% of the weight loss occurred below 200°C and the main weight loss happened at 400°C–500°C due to the decomposition of the frameworks. The X-ray diffraction (XRD) showed its amorphous structure (Fig. S5).

Fig. 2 shows the N_2 adsorption-desorption isotherms of the polymers. It exhibited a Type-IV profile [37], indicative of its hierarchical microporous and mesoporous character. The pore size distribution based on the non-local density functional theory model followed this analysis. The detected pores were mainly distributed in the range of 20–60 nm. As shown in Fig. S6, as the feeding amount of MA and TMA was close, the functional groups of MA and TMA were condensed for the formation of oligomers, and the oligomers further assembled to the polymers. As different feeding amount of MA and TMA was applied, some changes occurred for NTM1, NTM2, and NTM3 (Fig. S7). According to the N_2 isotherms, the structural parameters of the polymers were obtained and it is observed that NTM1, NTM2,

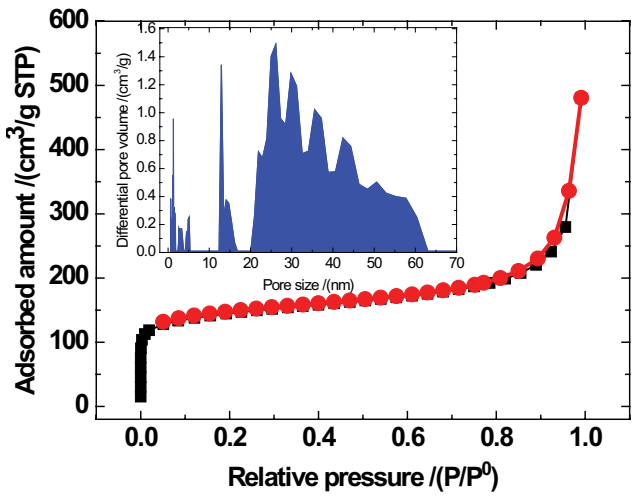

Fig. 2. N_2 adsorption–desorption isotherms and pore size distribution (inserted) of the polymers.

and NTM3 had the S_{BET} of 246, 487, and 463 m^2/g, respectively (Table 1), their total pore volume (V_{total}) were 0.95, 0.78, and 0.74 cm^3/g, respectively. As the ratio of MA/TMA increased, the S_{BET} increased first and then decreased. It can be explained by the fact that the collision probability of the activated molecules increased first as the ratio increased, inducing a sufficient amidation. Nevertheless, a higher ratio of the monomers resulted in an incomplete reaction. As a result, considerable amino groups were remained in the polymers. The weak acid capacity (C_a) and weak basic capacity (C_b) gave the same conclusion (Table S2). NTM3 with the highest ratio had the highest C_b (4.35 mmol/g). Meanwhile, the elemental analysis in Table S1 also clarified that NTM3 had the highest N content due to the residual amino groups. The SEM images in Figs. 3a and b show that the polymers were irregular spheres and plentiful interconnected macropores were existent for the polymers. The TEM images in Figs. 3c–f displayed that the particles were 40–80 nm with an amorphous structure. The polymers were composed of aggregated nanoparticles with alternately dark and bright microstructure.

3.2. Cd^{2+} adsorption

The equilibrium isotherms of Cd^{2+} were first measured for the polymers and Fig. 4a indicated that the q_e increased with increasing C_e. The Langmuir and Freundlich models were adopted for fitting the equilibrium data [38,39]. It can be seen from Table S3 that the correlation coefficients based on the Langmuir model (R_L^2) were higher than the latter (R_F^2), indicating that the Cd^{2+} adsorption was better described by the Langmuir model with a monolayer adsorption process. These results were accordant to the reported results in the literature [24–26]. In addition, the q_{max} on NTM1, NTM2, and NTM3 were predicted to be 326.3, 367.8, and 392.5 mg/g, respectively. NTM3 was proven the most efficient and its low S_{micro}/S_{BET} (57.5%) and the largest amino groups should be the direct cause. As compared to the q_{max} of Cd^{2+} on NTM3

Table 1
Structural parameters of the polymers

	S_{BET}/(m^2/g)	S_{micro}/(m^2/g)	S_{micro}/S_{BET}/(%)	V_{total}/(cm^3/g)	V_{micro}/(cm^3/g)	V_{micro}/V_{total}/(%)
NTM1	246	225	91	0.951	0	0
NTM2	487	273	56	0.785	0.144	17.9
NTM3	463	266	57	0.744	0.148	18.9

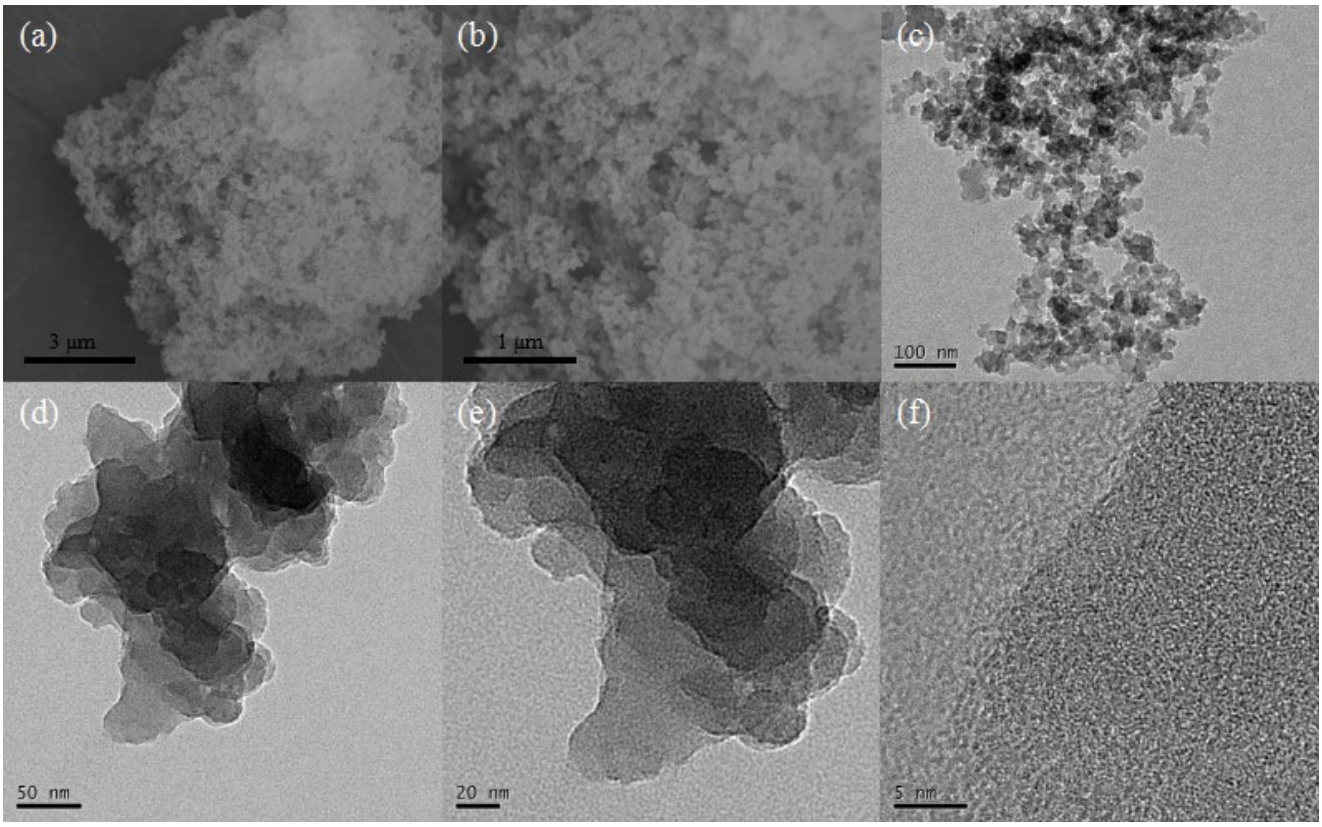

Fig. 3. (a-b) SEM and (c-f) TEM images of the polymers.

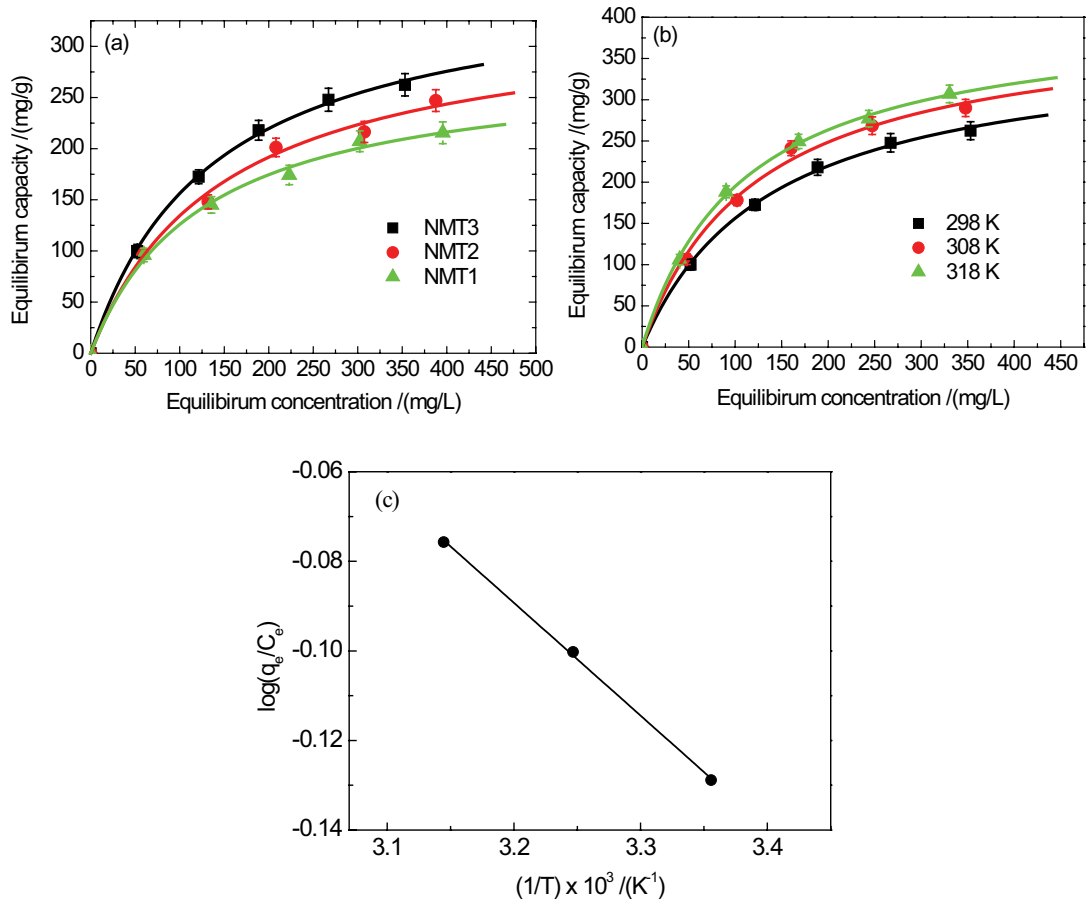

Fig. 4. Isotherms of Cd^{2+} adsorption on (a) NTM1, NTM2, and NTM3 (0.02 g of the polymers; 50 mL of Cd^{2+} aqueous solution; the initial concentration was 100–500 mg/L, T = 298 K), (b) NTM3 at 298, 308, and 318 K, and (c) Van't-Hoff plotting.

with some other sorbents reported in the literature (Table 2) [17,18,28,30,31,40–47], NTM3 was one of the most promising sorbents.

Subsequently, NTM3 was employed as the sorbent and the equilibrium isotherms were measured at 298, 308, and 318 K, respectively. Fig. 4b displayed that the q_e increased as the temperature increased, implying an endothermic process [36,48]. The fitted results in Table S4 gave similar information that the q_{max} increased with elevating the temperature. The Van't-Hoff equation was applied to figure out the thermodynamic parameters such as the adsorption enthalpy (ΔH, kJ/mol), entropy (ΔS, kJ/mol), and free energy (ΔG, J/(mol K)) [31,35,44],

$$\log\left(\frac{q_e}{C_e}\right) = -\frac{\Delta H}{2.303RT} + \frac{\Delta S}{2.303R} \quad (2)$$

The ΔH and ΔS were predicted by plotting the log (q_e/C_e) vs. $1/T$. As shown in Fig. 4c and Table S5, the ΔH and ΔS were calculated to be 4.82 kJ/mol and 13.73 J/(mol K), respectively, indicating the adsorption was endothermic [36]. The positive ΔS can be explained by the release of H_2O molecules around Cd^{2+} in aqueous solution [11]. Due to the solvation effect, Cd^{2+} exists as the form of hydrated Cd^{2+} surrounded by lots of H_2O molecules. As the adsorption proceeded, the amino groups interacted with Cd^{2+} and released abundant H_2O molecules and hence lead to the increased ΔS. The ΔG decreased with increasing the temperature, implying a more spontaneous process at a higher temperature.

Fig. 5 shows the q_e as a function of the solution pH. It is observed that the q_e increased first and then slightly decreased as the solution pH increased from 1.18 to 10.02 and the largest q_e located at pH = 6. Fig. 5 also depicts the specific speciation of Cd^{2+} as the solution pH varied from 1 to 14 by the Visual MINTEQ 3.0 software. At a lower solution pH, superfluous H^+ made the active sites such as the $–NH_2$, –NH–, and –C=O protonated, which was adverse for the adsorption. Of course the competition adsorption of H^+ was also a reason for the lower q_e [11]. At the solution pH increased, the active sites of the polymers were liberated, which had a strong chelating with Cd^{2+} [12]. When the solution pH was higher than 6, the precipitation of Cd^{2+} as the form of $Cd(OH)^+$ and $Cd(OH)_2$ appeared, affecting the q_e in a negative way [23].

Fig. 6 gives the kinetic curve of Cd^{2+} adsorption on the polymers. It is obvious that the adsorption was very fast at the beginning of 6 min and reached the equilibrium within 15 min. In the beginning, plentiful active sites were available for Cd^{2+} adsorption, which facilitated the strong affinity of

Table 2
Comparison of the q_{max} for Cd^{2+} adsorption on the sorbents

	A+dsorption conditions	q_{max} (mg/g)	Ref.
γ-Cyclodextrin/chitosan composites	pH = 8.5, T = 298 K	833.3	[17]
rGO-PDTC/Fe_3O_4	pH = 6.0, T = 298 K	179.8	[18]
Poly(itaconic acid)-grafted chitosan	pH = 6.0, T = 298 K	405.5	[28]
Schiff-based POPs	pH = 6.0, T = 298 K	89.60	[30]
Polyacrylic acid modified nanotrap	pH = 7.0, T = 298 K	406.6	[31]
Esterified grain	pH = 5.0, T = 298 K	473.9	[40]
Thiourea-modified chitosan	pH = 6.0, T = 298 K	256.4	[41]
Nano-PFM	pH = 6.0, T = 298 K	39.05	[42]
β-Cyclodextrin	pH = 6.0, T = 298 K	136.4	[43]
Activated carbon	pH = 8.0, T = 303 K	15.75	[44]
PAA-MMC	pH = 7.0, T = 303 K	406.6	[31]
UFMBO	pH = 6.0, T = 298 K	74.77	[45]
AA hydrogel	pH = 6.5, T = 298 K	495.0	[46]
Cashew nutshell	pH = 5.0, T = 298 K	436.7	[47]
NTM3	pH = 6.0, T = 298 K	392.5	This work

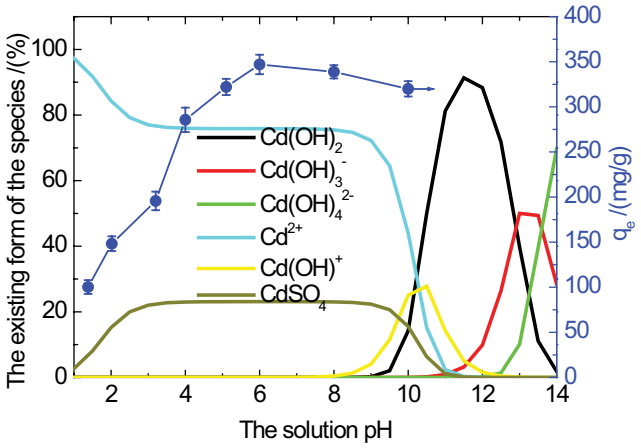

Fig. 5. q_e of Cd^{2+} on NTM3 as a function of the solution pH (0.02 g of the polymers; 50 mL of Cd^{2+} aqueous solution; the initial concentration Cd^{2+} was 5 mg/L, T = 298 K, pH = 2–10).

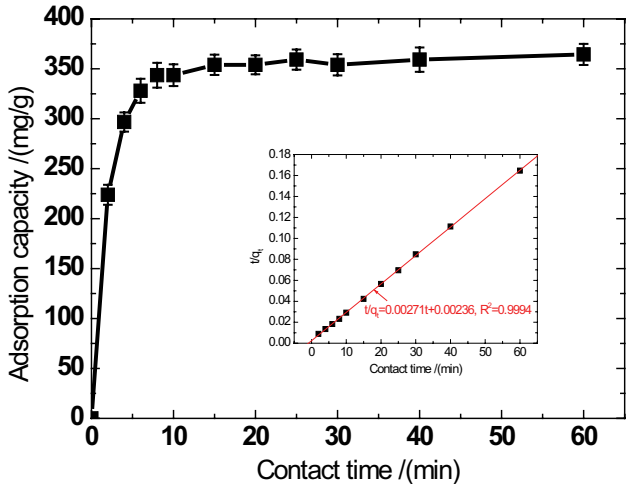

Fig. 6. Kinetic curve of Cd^{2+} adsorption on NTM3 (0.02 g of the polymers; 250 mL of Cd^{2+} aqueous solution; the initial concentration was 500 mg/L, T = 298 K).

Cd^{2+} to the polymers. As the adsorption proceeded, the available sites and the Cd^{2+} concentration were both reduced, making the adsorption rate dropped. The fast adsorption of Cd^{2+} on the polymers was shown to be superior to some other materials in the literature [49,50]. The pseudo-first-order and pseudo-second-order rate equations were applied for fitting the kinetic data [51,52] and the pseudo-second-order was better for characterizing the kinetic data since R^2 = 0.997. After the adsorption, the mixed desorption solvent including 1.0 mol/L of HCl and 0.5 mol/L of ethylene diamine tetraacetic acid (EDTA) was used for the regeneration of the polymers, 99.6% of the desorption efficiency was achieved. The polymers were used for six cycles and Fig. 7a displayed that the q_e had not a considerable loss. Additionally, the selectivity experiment was investigated in a mixed solution containing different metals such as K^+, Na^+, Ni^{2+}, Cu^{2+}, Mn^{2+}, Cd^{2+}, Ca^{2+}, Zn^{2+}, Mg^{2+}, Pb^{2+}, and Fe^{3+}. Fig. 7b demonstrates that the polymer exhibited significantly higher q_e for Cd^{2+} than some other metals.

To clarify the mechanism for Cd^{2+} adsorption on the polymers, the XPS spectra of the polymers before and after Cd^{2+} adsorption were tested. After Cd^{2+} adsorption, the C1s relevant to the carbonyl (C=O) shifted from 284.7 to 285.0 eV (Fig. 1b), the band correlated to the triazine ring (C=N) changed from 286.5 to 286.7 eV. However, there was no shift for the C=C configuration at 287.7 eV. Noticeably, Fig. 1c displays that the N1s related to triazine groups (C=N) changed from 398.3 to 398.6 eV after Cd^{2+} adsorption and the amino groups (–NH_2) with the binding energy at 399.5 eV was blue-shifted to 399.8 eV. Meanwhile, Fig. 1d indicates that the O1s correlated to the carbonyl (C=O) was shifted from 531.7 to 531.4 eV. The shift of the binding energy was strong evidence for the strong interaction between the active sites and Cd^{2+}.

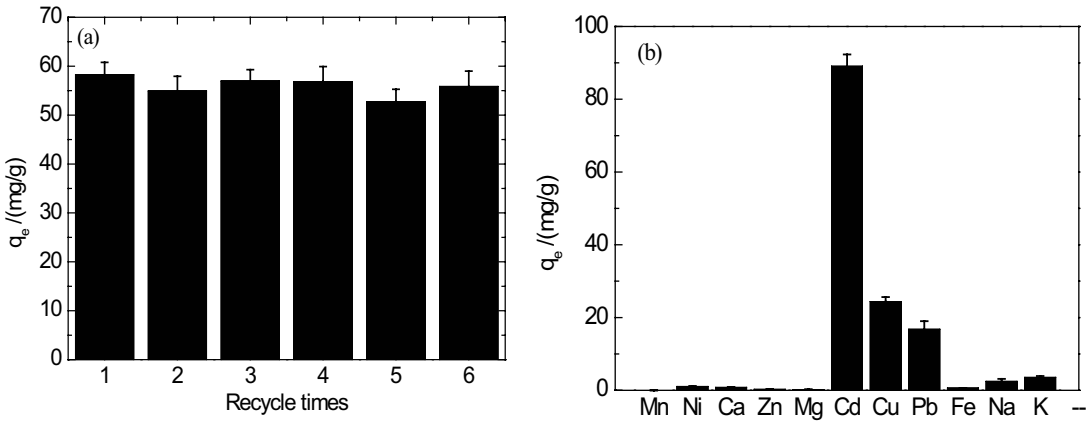

Fig. 7. (a) q_e of Cd^{2+} adsorption on NTM3 as a function of the repeated times (0.02 g of the polymers; 50 mL of Cd^{2+} aqueous solution; the initial concentration was 50 mg/L, T = 298 K), and (b) adsorption selectivity of NTM3 for Cd^{2+} (each ion have the initial concentration of 50 mg/L, T = 298 K).

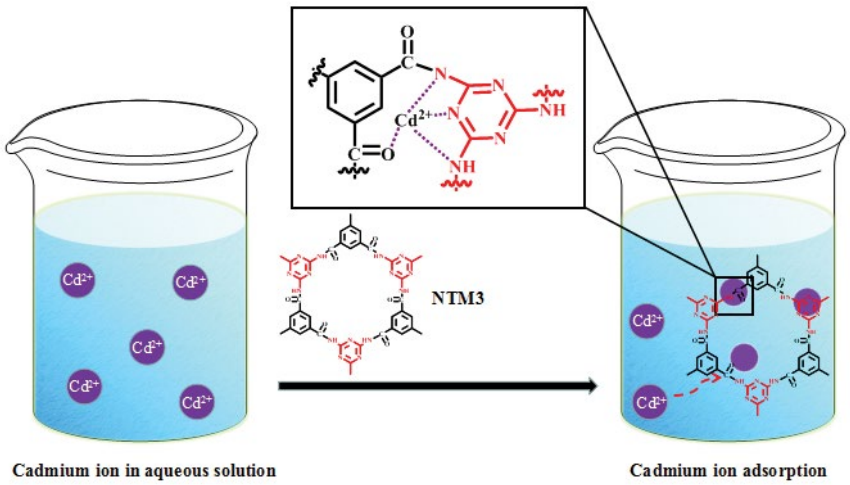

Fig. 8. Illustration of the chelating interaction between Cd^{2+} and the polymers.

As illustrated in Fig. 8, the N (from the amino, acylamino, and triazine) and the O (acylamino and carboxyl) of the polymers formed strong coordination complexes with Cd^{2+}. Therefore, it can be concluded that the embedded acylamino, triazine ring, and amino groups of the polymers formed stable coordination complexes with Cd^{2+} and the strong chelating lead to the efficient removal of Cd^{2+}.

4. Conclusion

The acylamino functionalized triazine-based POPs were easily fabricated using a one-pot amidation reaction and the polymers had tuned S_{BET} (246–463 m^2/g) and predominated mesopores. The polymers were efficient for Cd^{2+} adsorption with the q_{max} of 392.5 mg/g at pH = 6 and the acylamino groups were important for the adsorption due to the strong chelating of N and O with Cd^{2+}. Besides, the Cd^{2+} adsorption was very fast and less than 15 min was enough for the equilibrium. The polymers could be repeatedly used at least six cycles without significant loss of the q_e.

Acknowledgments

The National Natural Science Foundation of China (No. 51974374) is gratefully acknowledged for the financial supports.

References

[1] L. Ma, Q. Wang, S.M. Islam, Y. Liu, S. Ma, M.G. Kanatzidis, Highly selective and efficient removal of heavy metals by layered double hydroxide intercalated with the MoS_4^{2-} ion, J. Am. Chem. Soc., 138 (2016) 2858–2866.

[2] L.L. Ling, W.J. Liu, S. Zhang, H. Jiang, Magnesium oxide embedded nitrogen self-doped biochar composites fast and high-efficiency adsorption of heavy metals in an aqueous solution, Environ. Sci. Technol., 51 (2017) 10081–10089.

[3] H.F. Guo, X.L. Zhang, C.X. Kang, J. Zhang, Z.X. Xu, C.H. Jiang, P.Y. Luo, Z.F. Fu, M.N. Ding, Y.L. Lv, Synthesis of magnetic Fe-doped hydroxyapatite nanocages with highly efficient and selective adsorption for Cd^{2+}, Mater. Lett., 253 (2019) 144–147.

[4] Y. Shen, H. Li, W. Zhu, S.H. Ho, W. Yuan, J. Chen, Y. Xie, Microalgal biochar immobilized complex a novel efficient

biosorbent for cadmium removal from aqueous solution, Bioresour. Technol., 244 (2017) 1031–1038.
[5] Y. Kacar, C. Arpa, S. Tan, A. Denizli, O. Genc, M.Y. Arıca, Biosorption of Hg(II) and Cd(II) from aqueous solutions: comparison of biosorptive capacity of alginate and immobilized live and heat-inactivated *Phanerochaete chrysosporium*, Process Biochem., 37 (2002) 601–610.
[6] J. Liang, X.M. Li, Z.G. Yu, G.M. Zeng, Y. Luo, L.B. Jiang, Z.X. Yang, Y.Y. Qian, H.P. Wu, Amorphous MnO_2 modified biochar derived from aerobically composted swine manure for adsorption of Pb(II) and Cd(II), ACS Sustainable Chem. Eng., 5 (2017) 5049–5058.
[7] T.A. Saleh, A.A. Al-Saadi, Surface characterization and sorption efficacy of tire obtained carbon: an experimental and semiempirical study of rhodamine B adsorption, Surf. Interface Anal., 47 (2015) 785–792.
[8] L.Z. Wang, J.F. Guo, X.Y. Xiang, Y.F. Sang, J.H. Huang, Melamine-supported porous organic polymers for efficient CO_2 capture and Hg^{2+} removal, Chem. Eng. J., 387 (2020) 124070.
[9] A.O. Bello, B.S. Tawabini, A.B. Khalil, C.R. Boland, T.A. Saleh, Phytoremediation of cadmium-, lead- and nickel-contaminated water by *Phragmites australis* in hydroponic systems, Ecol. Eng., 120 (2018) 126–133.
[10] H.A. Sani, M.B. Ahmad, M.Z. Hussein, N.A. Ibrahim, T.A. Saleh, Nanocomposite of ZnO with montmorillonite for removal of lead and copper ions from aqueous solutions, Process Saf. Environ. Prot., 109 (2017) 97–105.
[11] K. Pyrzynska, Removal of cadmium from wastewaters with low-cost adsorbents, J. Environ. Chem. Eng., 7 (2019) 102795.
[12] Y.S. Fetisova, O.A. Dudarko, M. Bauman, A. Lobnik, V.V. Sliesarenko, Adsorption of lead(II), cadmium(II) and dysprosium(III) from aqueous solutions using mesoporous silica modified with phosphonic acid groups, J. Sol-Gel Sci. Technol., 206 (2018) 199–207.
[13] B.M. Babic, S.K. Milonjic, M.J. Polovina, S. Cupic, B.V. Kaludjerovic, Adsorption of zinc, cadmium and mercury ions from aqueous solutions on an activated carbon cloth, Carbon, 40 (2002) 1109–1115.
[14] Y. Shin, G.E. Fryxell, W. Um, K. Parker, S.V. Mattigod, R. Skaggs, Sulfur-functionalized mesoporous carbon, Adv. Funct. Mater., 17 (2007) 2897–2901.
[15] M. Naushad, T. Ahamad, B.M. Al-Maswari, A.A. Alqadami, S.M. Alshehri, Nickel ferrite bearing nitrogen-doped mesoporous carbon as an efficient adsorbent for the removal of highly toxic metal ion from aqueous medium, Chem. Eng. J., 330 (2017) 1351–1360.
[16] A. Shahat, Md. R. Awual, Md. A. Khaleque, Md. Z. Alam, Mu. Naushad, A.M.S. Chowdhury, Large-pore diameter nano-adsorbent and its application for rapid lead(II) detection and removal from aqueous media, Chem. Eng. J., 273 (2015) 286–295.
[17] A.K. Mishra, A.K. Sharma, Synthesis of γ-cyclodextrin/chitosan composities for the efficient removal of Cd(II) from aqueous solution, Int. J. Biol. Macromol., 49 (2011) 504–512.
[18] W. Fu, Z.Q. Huang, Magnetic dithiocarbamate functionalized reduced graphene oxide for the removal of Cu(II), Cd(II), Pb(II), and Hg(II) ions from aqueous solution: synthesis, adsorption, and regeneration, Chemosphere, 209 (2018) 449–456.
[19] S.Z. Guo, K.L. Wu, Y. Gao, L.H. Liu, X.X. Zhu, X.L. Li, F. Zhang, Efficient removal of Zn(II), Pb(II), and Cd(II) in wastewater based on magnetic graphitic carbon nitride materials with enhanced adsorption capacity, J. Chem. Eng., 63 (2018) 3902–3912.
[20] Z. Liu, G. Chen, F. Zhou, J.H. Huang, Imidazolium salt incorporated poly(N-vinylimidazole-co-ethylene glycol dimethacrylate) for efficient adsorption of congo red and Hg^{2+} from aqueous solution, J. Chem. Eng. Data, 64 (2019) 2627–2633.
[21] M. Naushad, S. Vasudevan, G. Sharma, A. Kumar, Z.A. Alothman, Adsorption kinetics, isotherms, and thermodynamic studies for Hg^{2+} adsorption from aqueous medium using alizarin red-S-loaded amberlite IRA-400 resin, Desal. Water Treat., 57 (2016) 18551–18559.
[22] M. Naushad, Surfactant assisted nano-composite cation exchanger: development, characterization and applications for the removal of toxic Pb^{2+} from the aqueous medium, Chem. Eng. J., 235 (2014) 100–108.
[23] B. Aguila, Q. Sun, J. Perman, L. Earl, C. Abney, R. Elzein, R. Schlaf, S.Q. Ma, Efficient mercury capture using functionalized porous organic polymer, Adv. Mater., 29 (2018) 31.
[24] L.S. Shao, M.Q. Liu, Y.F. Sang, J.H. Huang, One-pot synthesis of melamine-based porous polyamides for CO_2 capture, Microporous Mesoporous Mater., 285 (2019) 105–111.
[25] X.M. Wang, H. Ou, J.H. Huang, One-pot synthesis of hyper-cross-linked polymers chemically modified with pyrrole, furan, and thiophene for phenol adsorption from aqueous solution, J. Colloid Interface Sci., 538 (2019) 499–506.
[26] M.B. Feng, P. Zhang, H.C. Zhou, V.K. Sharma, Water-stable metal-organic frameworks for aqueous removal of heavy metals and radionuclides: a review, Chemosphere, 209 (2018) 783–800.
[27] Y.F. Sang, J.H. Huang, Benzimidazole-based hyper-cross-linked poly(ionic liquid)s for efficient CO_2 capture and conversion, Chem. Eng. J., 385 (2020) 123973.
[28] G.Z. Kyzas, P.I. Siafaka, D.A. Lambropoulou, N.K. Lazaridis, D.N. Bikiaris, Poly (itaconic acid)-grafted chitosan adsorbents with different cross-linking for Pb(II) and Cd(II) uptake, Langmuir, 30 (2013) 120–131.
[29] R. Karthik, Removal of Pb(II) and Cd(II) ions from aqueous solution using polyaniline grafted chitosan, Chem. Eng. J., 263 (2015) 168–177.
[30] J.J. Zhao, Y.Z. Niu, B. Ren, H. Chen, S.X. Chen, J. Jin, Y. Zhang, Synthesis of Schiff base functionalized superparamagnetic Fe_3O_4 composites for effective removal of Pb(II) and Cd(II) from aqueous solution, Chem. Eng. J., 347 (2018) 574–584.
[31] G.M. Zeng, Y.Y. Liu, L. Tang, G.D. Yang, Y. Pang, Y. Zhang, Y.Y. Zhou, Z. Li, M.Y. Li, M.Y. Lai, Enhancement of Cd(II) adsorption by polyacrylic acid-modified magnetic mesoporous carbon, Chem. Eng. J., 259 (2015) 163–170.
[32] T.A. Saleh, Simultaneous adsorptive desulfurization of diesel fuel over bimetallic nanoparticles loaded on activated carbon, J. Cleaner Prod., 172 (2018) 2123–2132.
[33] O.S. Taskin, N. Ersoy, A. Aksu, B. Kiskan, N. Balkis, Y. Yagci, Melamine-based microporous polymer for highly efficient removal of copper(II) from aqueous solution, Polym. Int., 65 (2016) 439–445.
[34] Y. He, Q.Q. Liu, F. Liu, C.S. Huang, C.J. Peng, Q. Yang, H.L. Wang, J. Hu, H.L. Liu, Porous organic polymer bifunctionalized with triazine and thiophene groups as a novel adsorbent for removing Cu(II), Microporous Mesoporous Mater., 233 (2016) 10–15.
[35] R.X. Peng, G. Chen, F. Zhou, R.L. Man, J.H. Huang, Catalyst-free synthesis of triazine-based porous organic polymers for Hg^{2+} adsorptive removal from aqueous solution, Chem. Eng. J., 371 (2019) 260–266.
[36] T.A. Saleh, Nanocomposite of carbon nanotubes/silica nanoparticles and their use for adsorption of Pb(II): from surface properties to sorption mechanism, Desal. Water Treat., 57 (2015) 10730–10744.
[37] M. Thommes, K. Kaneko, A.V. Neimark, J.P. Olivier, F. Rodriguez-Reinoso, J. Rouquerol, K.S.W. Sing, Physisorption of gases, with special reference to the evaluation of surface area and pore size distribution (IUPAC technical report), Pure Appl. Chem., 87 (2015) 1051–1069.
[38] I. Langmuir, The constitution and fundamental properties of solids and liquids Part I. solids, J. Am. Chem. Soc., 38 (1916) 2221–2295.
[39] H.M.F. Freundlich, Over the adsorption in solution, J. Phys. Chem., 57 (1906) 1100–1107.
[40] Q. Li, L. Chai, W. Qin, Cadmium(II) adsorption on esterified spent grain: equilibrium modeling and possible mechanisms, Chem. Eng. J., 197 (2012) 173–180.
[41] A. Chen, G. Zeng, G. Chen, X. Hu, M. Yan, S. Guan, C. Shang, L. Lu, Z. Zhou, G. Xie, Novel thiourea-modified magnetic ion-imprinted chitosan/TiO_2 composite for simultaneous removal of cadmium and 2,4,-dichlorophenol, Chem. Eng. J., 191 (2012) 85–94.
[42] Z.M. Liu, X. Li, P. Zhan, F.P. Hu, X. Ye, Removal of cadmium and copper from water by a magnetic adsorbent of PFM:

adsorption performance and microstructural morphology, Sep. Purif. Technol., 206 (2018) 199–207.
[43] J.Y. He, Y.L. Li, C.M. Wang, K.S. Zhang, D.Y. Lin, L.T. Kong, J.H. Liu, Rapid adsorption of Pb, Cu, and Cd from aqueous solutions by β-cyclodextrin polymers, Appl. Surf. Sci., 426 (2017) 29–39.
[44] M. Madhava Rao, D.K. Ramana, K. Seshaiah, M.C. Wang, S.W. Chang, Removal of some metal ions by activated carbon prepared from *Phaseolus aureus* hulls, J. Hazard. Mater., 166 (2009) 1006–1013.
[45] L.B. Zhong, J. Yin, S.G. Liu, Q. Liu, Y.S. Yang, Y.M. Zheng, Facile one-pot synthesis of urchin-like Fe-Mn binary oxide nanoparticles for effective adsorption of Cd(II) from water, RSC Adv., 6 (2016) 103438–103445.
[46] X.W. Peng, L.X. Zhong, J.L. Ren, R.C. Sun, Highly effective adsorption of heavy metal ions from aqueous solutions by macroporous xylan-rich hemicelluloses-based hydrogel, J. Agric. Food Chem., 6 (2012) 3909–3916.
[47] P.S. Kumar, S. Ramalingam, R.V. Abhinaya, S.D. Kirupha, A. Murugesan, S. Sivanesan, Adsorption of metal ions onto the chemically modified agricultural waste, Clean-Soil Air Water, 40 (2012) 188–197.
[48] Y.Q. Gan, G. Chen, Y.F. Sang, F. Zhou, R.L. Man, J.H. Huang, Oxygen-rich hyper-cross-linked polymers with hierarchical porosity for aniline adsorption, Chem. Eng. J., 368 (2019) 29–36.
[49] V.K. Gupta, A. Nayak, Cadmium removal and recovery from aqueous solutions by novel adsorbents prepared from orange peel and Fe_2O_3 nanoparticles, Chem. Eng. J., 180 (2012) 81–90.
[50] M. Torab-Mostaedi, M. Asadollahzadeh, A. Hemmati, A. Khosravi, Equilibrium, kinetic, and thermodynamic studies for biosorption of cadmium and nickel on grapefruit peel, J. Taiwan Inst. Chem. Eng., 44 (2013) 295–302.
[51] S. Lagergren, About the theory of so-called adsorption of soluble substances, Kungliga Svenska Vetenskapsakademiens, Handlingar, 24 (1898) 1–39.
[52] Y.S. Ho, Review of second-order models for adsorption systems, J. Hazard. Mater., 136 (2006) 681–689.

Supplementary materials

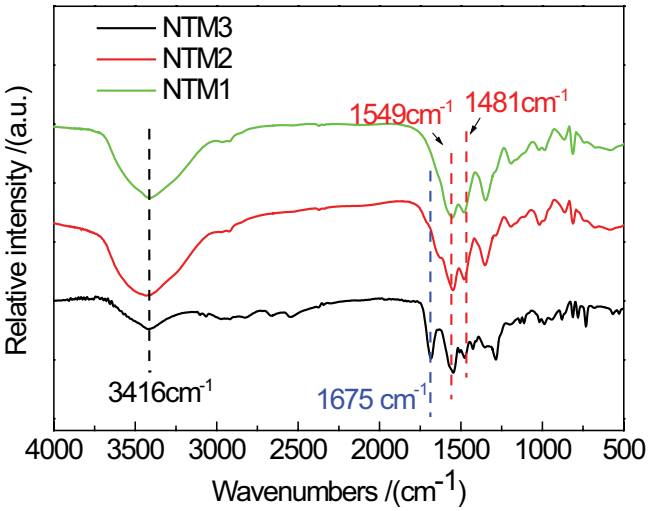

Fig. S1. FT-IR spectra of NTM1, NTM2, and NTM3.

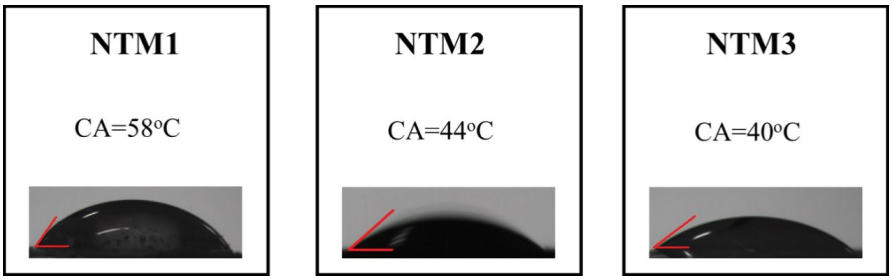

Fig. S2. Contact angle of NTM1, NTM2, and NTM3.

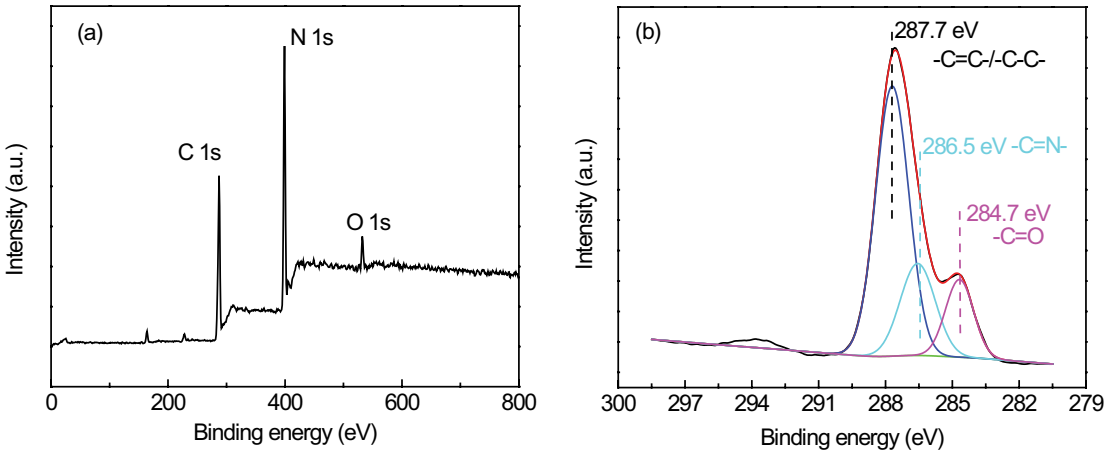

Fig. S3. XPS spectra of NTM2 (a) survey and (b) C 1s.

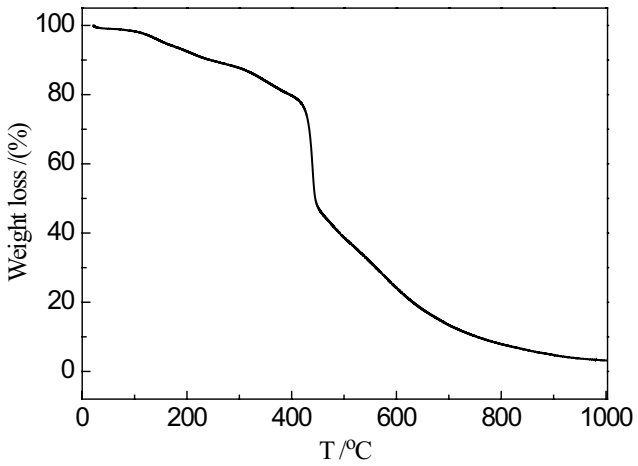

Fig. S4. TGA curve of NTM3.

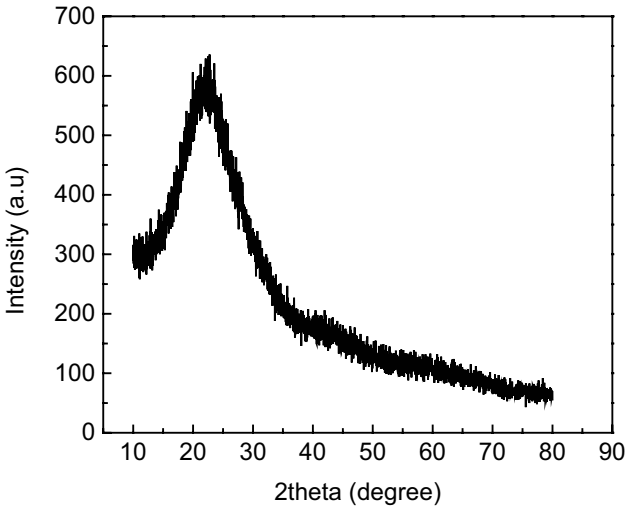

Fig. S5. XRD pattern of NTM3.

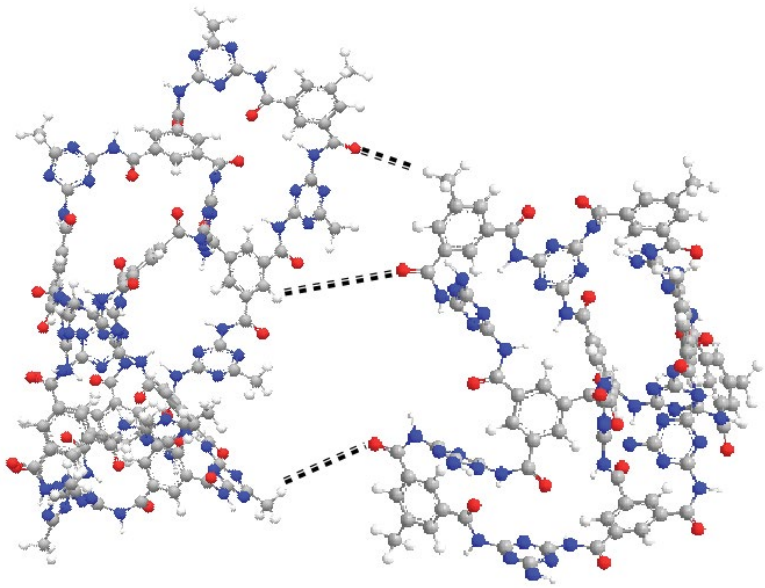

Fig. S6. Prediction of the pore formation mechanism of the polymers.

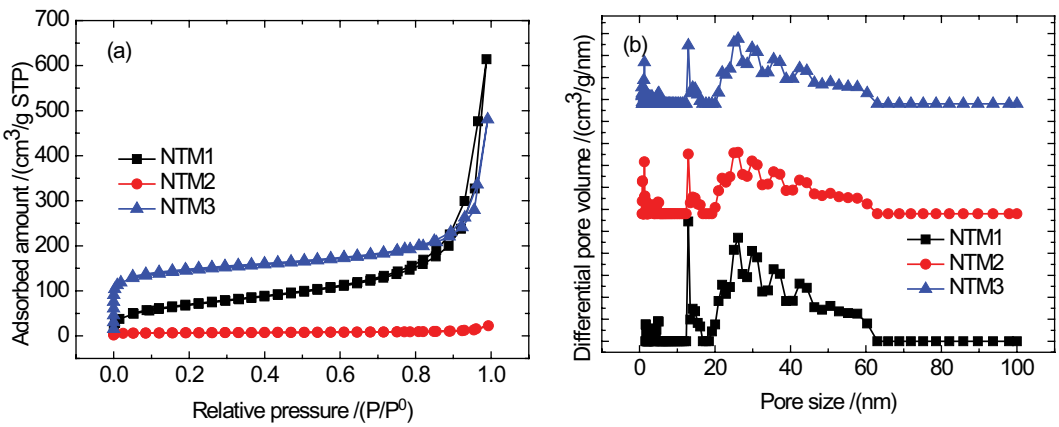

Fig. S7. N_2 adsorption–desorption isotherms and pore size distribution of the polymers.

Table S1
Elemental analysis of the polymers

	C/(wt.%)	N/(wt.%)	H/(wt.%)	S/(wt.%)	O calculated/(wt.%)
NTM1	44.7	32.6	5.4	2.1	15.2
NTM2	40.3	36.2	5.3	2.6	15.6
NTM3	34.6	40.9	5.2	2.4	16.9

Table S2
Weak acid capacity (C_a) and weak basic capacity (C_b) of the polymers

	NTM1	NTM2	NTM3
C_a/(mmol/g)	0.68	0.55	0.31
C_b/(mmol/g)	1.23	2.33	4.35

Table S3
Correlative parameters for the adsorption of Cd^{2+} on NTM1, NTM2, and NTM3 according to the Langmuir model and Freundlich models

	Langmuir model			Freundlich model		
	K_L/(L/mg)	q_m/(mg/g)	R_L^2	K_F/((mg/g)(L/mg)$^{1/n}$)	n	R_F^2
NTM1	2.28×10^{-3}	326.3	0.9850	2.32	1.41	0.9492
NTM2	3.95×10^{-3}	367.8	0.9824	6.39	1.66	0.9650
NTM3	6.06×10^{-3}	392.5	0.9914	14.72	2.00	0.9845

Table S4
Correlative parameters for the adsorption of Cd^{2+} on NTM3 at 298, 308, and 318 K according to the Langmuir model and Freundlich models

	Langmuir model			Freundlich model		
	K_L/(L/mg)	q_m/(mg/g)	R_L^2	K_F/((mg/g)(L/mg)$^{1/n}$)	n	R_F^2
298 K	6.06×10^{-3}	392.5	0.9914	14.72	2.00	0.9845
308 K	7.52×10^{-3}	405.7	0.9988	16.28	2.32	0.9877
318 K	9.32×10^{-3}	431.2	0.9979	17.02	2.55	0.9898

Table S5
Thermodynamic parameters for the adsorptive removal of Cd^{2+} by the polymers

	Temperature/(K)	ΔG/(kJ/mol)	ΔS/(kJ/(mol K))	ΔH/(kJ/mol)	R^2
	298	0.73			
Cd^{2+}	308	0.59	13.73	4.82	0.9986
	318	0.46			